Self-Organization of Lipid-Porphyrin Conjugates at the Air/Water Interface

Paul Cressey, Wasim Abuillan, Nada Ibrahim, Jana Alhoussein, Oleg Konovalov, Gang Zheng, Ali Makky

Self-Organization of Lipid-Porphyrin Conjugates at the Air/Water interface

Dr. Paul Cressey[a], Dr.Wasim Abuillan[b], Dr. Nada Ibrahim[a,c], Jana Alhoussein[a], Dr. Oleg Konovalov[d], Prof. Dr. Gang Zheng[e,f] and Dr. Ali Makky[a] *

[a] Université Paris-Saclay, CNRS, Institut Galien Paris-Saclay, 92296, Châtenay-Malabry, France

[b] Physical Chemistry of Biosystems, Physical Chemistry Institute, University of Heidelberg, 69120 Heidelberg, Germany

[c] IMESCIA, Faculté de Pharmacie, 92296, Châtenay-Malabry, France

[d] European Synchrotron Radiation Facility (ESRF), Grenoble, 38043, France

[e] Princess Margaret Cancer Centre, University Health Network, 101 College Street, PMCRT 5-354, Toronto, Ontario M5G 1L7, Canada.

[f] Department of Medical Biophysics, University of Toronto, 101 College St., Toronto, ON M5G 1L7, Canada

* Corresponding author: ali.makky@universite-paris-saclay.fr, https://www.umr-cnrs8612.universite-paris-saclay.fr/index.php

Abstract

Lipid-porphyrin conjugates are versatile compounds which can self-assemble into liposome-like structures with multifunctional properties. Most of the conjugates that have been described so far, consisted in grafting pyropheophorbide-a (Pyro-a) or other porphyrin derivatives through the esterification of the hydroxyl group in the sn-2 position of a lysophosphatidylcholine. However, despite the versatility of these conjugates, less is known about the impact of the lipid backbone structure on their 2D phase behavior at the air/water interface and more precisely on their fine structures normal to the interface as well as on their in-plane organization. Herein, we synthesized a new lipid-porphyrin conjugate (PyroLSM) based on the amide coupling of Pyro-a to a lysosphingomyelin backbone (LSM) and we compared its interfacial behavior to that of Pyro-a and Pyro-a conjugated lysophosphatidylcholine (PyroLPC) using Langmuir balance

combined to a variety of other physical techniques. Our results provided evidence on the significant impact of the lipid backbone on the lateral packing of the conjugates as well as on the shape and size of the formed domains. Compared to Pyro-a and PyroLPC monolayers, PyroLSM exhibited the highest lateral packing which highlights the role of the lipid backbone in controlling their 2D organization which in turn may impact the photophysical properties of their assemblies.

Keywords: Lipid-porphyrin conjugates, air/water interface, XRR, GISAXS, domains.

Introduction

Lipid-porphyrin conjugates have gained recently tremendous attention for the development of multifunctional nanomaterials with light activatable properties. These unique building blocks can self-assemble in aqueous media into liposome-like structures either by their own or when mixed with helper phospholipids such as cholesterol. Compared to their disassembled counterparts, the lipid-porphyrin assemblies exhibit unique photophysical properties and biomedical outcomes.[1] In these assemblies, the porphyrin cores adopt a densely packed arrangement which quenches their fluorescence ability. Thus, upon their illumination at their absorbance wavelengths, the absorbed photonic energy is dissipated thermally through vibrational relaxation.[2] This leads to the generation of heat upon the illumination of the lipid-porphyrin assemblies.[2-4] Therefore, the nanoassemblies may act as highly efficient cytotoxic photothermal agent and can be used in photothermal therapy (PTT).[4] Interestingly, once the liposomal structures are passively disrupted in the body, both the fluorescence and photosensitizing properties of porphyrin pigments are regenerated thus enabling another phototherapeutic modality called photodynamic therapy (PDT).[2, 5] Most of the lipid-porphyrin conjugates that have been described so far for PTT/PDT and photoacoustic imaging applications

were usually synthesized through esterification of the sn-2 position of lysophosphatidylcholine (LPC) with either pyropheophorbide-a (Pyro-a),[2] bacteriochlorophyll a [2] or benzoporphyrin derivative. [6, 7] PyroLPC also named Pyrolipid [2] which consists in conjugating Pyro-a directly to LPC, is the most successful conjugate reported to date. Indeed, the PyroLPC conjugates were shown to form stable supramolecular assemblies with multifunctional properties. [2] Other conjugates consisting of either pheophorbide-a[8] (Ph_xLPC) or pyropheophorbide-a[2] (Pyr_xLPC) coupled to the hydroxyl group in the sn-2 position of LPC via different linkers exhibiting different lengths have also been described in our previous works.[9-12] Compared to pheophorbide-a conjugated phospholipids (Ph_xLPC) which formed monolayers in the liquid expanded state, the Pyr_xLPC compounds formed films in the liquid-condensed state with subsequent appearance of well structured domains at the air/water interface.[11] This highlighted the importance of π-π interactions between the Pyro-a chromophores in dictating the organization of the conjugates at the air/water interface[11] and thus their self-assembling properties when suspended in water.[12] Besides LPC backbone, lysosphingomyelin (LSM) has also been employed. LSM based conjugates exhibited promising properties in favoring the assemblies of conjugated porphyrins into liposome-like structures [9, 10, 13] with multifunctional properties. Nevertheless, despite the versatility of these lipid-porphyrin conjugates, less is known about the impact of lipid backbone on their 2D phase behavior at the air/water interface and more precisely on their fine structures normal to the interface as well as on their in-plane organization. Herein, we synthesized a new lipid-porphyrin conjugate based on the amide coupling of Pyro-a to a LSM backbone,[9, 10, 13] referred in this work as the PyroLSM conjugate. The 2D phase behavior of Pyro-a, PyroLSM and PyroLPC was assessed at the air/water interface using a Langmuir balance. The morphology of the monolayers was thoroughly studied using Brewster angle microscopy

(BAM) and atomic force microscopy (AFM) on Langmuir-Blodgett transferred films. In addition, the fine structures of the monolayers were studied at the air/water interface by X-ray reflectometry (XRR) and Grazing-Incidence Small-Angle X-ray Scattering (GISAXS).

Experimental Section

Materials

Pyropheophorbide-a (Pyro-a, ≥ 95%, Mw = 534.66 g/mol) was purchased from Livchem Logistics GmbH (Frankfurt, Germany). Egg sphingomyelin (Egg SM, 99%, Mw=710.965 g.mol^{-1}) was purchased from Avanti Polar Lipids (Alabaster, AL). N-(3-Dimethylaminopropyl)-N′-ethyl carbodiimide hydrochloride (EDC.HCl, 99%, Mw= 191.70 gmol^{-1}) 1-hydroxybenzotriazole hydrate (HOBt, 97%, Mw= 135.12 gmol^{-1}), triethylamine (TEA, 99%, Mw= 101.19 g.mol^{-1}), HEPES (99.5%, Mw= 238.31 gmol^{-1}), sodium chloride (NaCl, 99%, Mw= 58.44 g.mol^{-1}), methanolic hydrogen chloride (0.5M) were provided by Sigma (St. Louis,MO, USA). The ultrapure water (γ = 72.2 mN/m at 22° C) used in all experiments was produced by a Millipore Milli-Q® Direct 8 water purification system, with a resistivity of 18.2 MΩ.cm. Solvents were purchased from CARLO ERBA Reagents (Val de Reuil, France). All compounds and solvents were used without further purification. The synthesis of lysosphingomyelin (LSM) was carried out according to the previously reported procedure. [9] PyroLPC (also named Pyrolipid [2]) was supplied by Gang Zheng's lab.

Synthesis of PyroLSM

The lysosphingomylein (LSM) was prepared by acidic hydrolysis of egg sphingomyelin (N-hexadecanoyl-d-erythro-sphingosylphosphorylcholine) in anhydrous methanolic hydrogen chloride at 50 °C (Scheme S1) following the procedure described previously.[9] Pyro-a (48 mg,

0.09 mmol), EDC.HCl (24 mg, 0.12 mmol) and HOBt (17 mg, 0.12 mmol) were mixed in 2 mL of anhydrous choloform and stirred for 1 hour at room temperature under Argon, in the dark. LSM (40 mg, 0.08 mmol) was dissolved in 2 ml of anhydrous chloroform with 0.2 mL of TEA, and then added to the pyro-a/ EDC.HCl mixture, and stirred in the dark, at room temperature, under Argon for 24 hours. Chloroform was then removed under vacuum. The crude was resuspended in minimum amount of chloroform and purified by chromatography on silica gel (eluted with chloroform-methanol-ammonia 70:30:4, volume ratio; Rf=0.3). PyroLSM was obtained (21 mg, dark green powder, yield 26%).^{1}H NMR (DMSO-d_6, 300 MHz) δ 9.56 (s, 1H), 9.28 (s, 1H), 8.83 (s, 1H), 8.26 (d, *J* = 8.5 Hz, 1H), 8.09 (dd, *J* = 17.8, 11.7 Hz, 1H), 6.21 (dd, *J* = 46.3, 15.3 Hz, 2H), 6.09 (s, 1H), 5.62 – 5.34 (m, 2H), 5.13 (dd, *J* = 65.0, 20.4 Hz, 2H), 4.54 (d, *J* = 7.0 Hz, 1H), 4.22 – 3.92 (m, 6H), 3.71 (d, *J* = 9.0 Hz, 2H), 3.55 (s, 5H), 3.37 (s, 3H), 3.15 (s, 9H), 3.11 (s, 3H), 2.89 (dd, *J* = 15.8, 8.1 Hz, 1H), 2.66 (t, *J* = 20.2 Hz, 2H), 2.28 (s, 2H), 1.79 (d, *J* = 7.1 Hz, 3H), 1.57 (t, *J* = 7.4 Hz, 3H), 1.14 – 0.14 (m, 25H), -2.03 (s, 1H).;^{13}CNMR (DMSO-d_6,75 MHz) ; δ 195.64 (s), 172.68 (s), 171.86 (s), 162.24 (s), 154.52 (s), 150.47 (s), 148.46 (s), 145.06 (s), 141.18 (s), 137.65 (s), 136.26 (s), 135.67 (s), 135.36 (s), 132.06 (s), 131.65 (s), 130.90 (s), 130.44 (s), 129.46 (s), 128.19 (s), 123.06 (s), 106.29 (s), 104.42 (d, *J* = 11.0 Hz), 96.85 (s), 90.45 (d, *J* = 569.4 Hz), 70.00 (s), 66.00 (s, *J* = 5.6 Hz), 65.93 (s), 64.30 (s), 58.85 (s), 58.79 (s), 55.19 (s), 53.63 (s), 51.89 (s), 50.26 (s), 48.06 (s), 45.91 (s), 43.30 (s), 33.64 (s), 32.04 (s), 31.74 (s), 31.55 (s), 29.12 – 28.60 (m), 23.39 (s), 22.39 (s), 19.02 (s), 17.79 (s), 14.26 (s), 12.33 (s), 12.03 (s), 11.22 (s).MS (MALDI-TOF) for $[C_{56}H_{81}N_6O_7P]^+$; calculated: 981.59 $[M+H]^+$; observed; 981.59 $[M+H]^+$.

Surface Pressure Measurements

Pressure-area (π-A) isotherms of the pure components were recorded using a thermostated KSV-Nima Langmuir film balance (Biolin Scientific, Finland), composed of a Teflon trough (775.75 cm^2) equipped with two 145 mm long Delrin barriers. Fresh solutions of Pyro a and its derivatives at a concentration of 1 mg/ml in chloroform/methanol (9:1) were prepared. Then, 50 µL of Pyro a, 100 µL of PyroLSM or 80 µL of PyroLPC solutions were spread (~5×10^{16} to 6×10^{16} molecules) onto aqueous HEPES buffer solution (10 mM HEPES, 150 mM NaCl, pH = 7.4). After deposition, the solvents were left to evaporate for 15 min before compression of the monolayer at a rate of 10 $Å^2$/molecule/min. All experiments were performed at 22±1 °C and the results reported are mean values of at least three measurements. From the surface pressure−area data, the surface compressional moduli (K or Cs^{-1}) of monolayers were calculated, using Eq. 1 with A the molecular area and π, the surface pressure:

$$K = -A\left(\frac{\partial \pi}{\partial A}\right)_T \qquad \textit{(Eq. 1)}$$

Brewster Angle Microscopy (BAM)

The morphology of the lipid-porphyrin monolayers at the air/buffer interface was monitored using a Brewster angle microscope (Micro-BAM 3, NimaTechnology Ltd, Coventry, UK) mounted on a Langmuir trough. The microscope was equipped with a single frequency laser diode (λ = 659 nm, 30 mW optical power) generating a collimated beam of approximately 6 mm diameter, with a p-polarizer, analyzer, and a USB camera. The refracted beam was absorbed by a black glass plate placed in the subphase. The field of view of BAM was 3.6 × 4.1 mm^2. The image size was rescaled and the zone of interest was cropped using imageJ software to get a final image size of 2.0 × 2.0 mm^2 with a resolution of 5.6 µm/pixel.

Langmuir-Blodgett Transfer and Atomic Force Microscopy (AFM) Imaging

The Langmuir–Blodgett (LB) film transfer of the lipid-porphyrin monolayers was performed on freshly cleaved mica surfaces (1.5 × 1.5 cm^2) using the Langmuir trough equipped with a Teflon well. The freshly cleaved mica substrate was immersed into the buffer subphase, and then the corresponding lipid-porphyrin conjugate solution was spread (total number of spread molecules ~ 5×10^{16}) onto the subphase. After solvent evaporation, the monolayer was compressed at a constant rate (10 $Å^2$/molecule/min) and the pressure-area (π-A) isotherm was simultaneously recorded. When the surface pressure of 30 mN/m was reached, it was maintained constant and the mica substrate (1.5×1.5 cm^2) was lifted from the subphase at a speed of 1 mm/min. The transfer ratio [14] which is defined as the ratio between the decrease in the monolayer area during the deposition stroke and the surface area of the substrate was close to 1 (0.93 for Pyro-a; 0.92 for PyroLPC and 0.94 for PyroLSM). This indicates that the films are almost perfectly transferred onto the mica substrates. Afterwards, atomic force microscopy (AFM) imaging of the transferred lipid-porphyrin films was performed in ambient conditions at room temperature using a JPK Nanowizard Ultraspeed atomic force microscope from JPK Instruments (Berlin, Germany) in amplitude modulation AFM (AM-AFM) with force settings comprised between 60–65% of the free amplitude A ~12 nm. Gold-coated silicon ACTG cantilevers (nominal spring constant ~ 37 nN/nm, tip radius < 10 nm) from AppNano (Mountain View, CA) were used. For each transferred film, different regions of the mica substrate were systematically imaged at high resolution (5× 5 μm^2, 10 × 10 μm^2 and 15 × 15 μm^2 at 1024 × 1024 pixels) with the AFM. AFM images were then processed using the JPK-SPM Data Processing software (version 6.1.131). All AFM images were flattened by subtracting a polynomial fit from each scan line at a 2^{nd} regression order.

Synchrotron X-ray Experiments

X-ray experiments were carried out at the beamline ID10 of the European Synchrotron Radiation Facility (ESRF, Grenoble, France). The samples were irradiated with a monochromatic synchrotron beam with an energy of 8 keV (λ = 1.55 Å). The experiments were performed on monolayers of lipid-porphyrin conjugates spread on the surface of HEPES buffer (HEPES 10 mM, NaCl 150 mM, pH 7.4) and compressed to a surface pressure of 30 mN/m at a temperature of 293 K. The film balance was kept in a helium atmosphere to minimize air scattering and maintain consistent environment for all measurements.

Specular X-ray Reflectivity (XRR): XRR was measured with a MAXIPIX 2D detector (Multichip Area X-ray detector based on a photon-counting Pixel array).[15] The error bars in the XRR curves correspond to the error resulting from the counting statistics and were calculated as described previously.[16] After background subtraction, the specular reflectivity was analyzed using a genetic minimization algorithm implemented in the MOTOFIT software package [17] by choosing a two-slab model.[11]

Grazing Incidence Small Angle Scattering (GISAXS): The out-off specular plane scattered intensity were collected with a MAXIPIX 2D detector. The intensity from direct beam (0.1×2 mm^2) was blocked using a beam stop. The beam impinges on the sample at angle of incidence of α_c = 0.125° which close to the critical angle of total external reflection (α_c = 0.11°). Under these conditions, the beam footprint is estimated to be 92 mm^2. From the experimental geometry considerations, the GISAXS signal is translated into reciprocal space map[18] (supporting information, Figure S1).

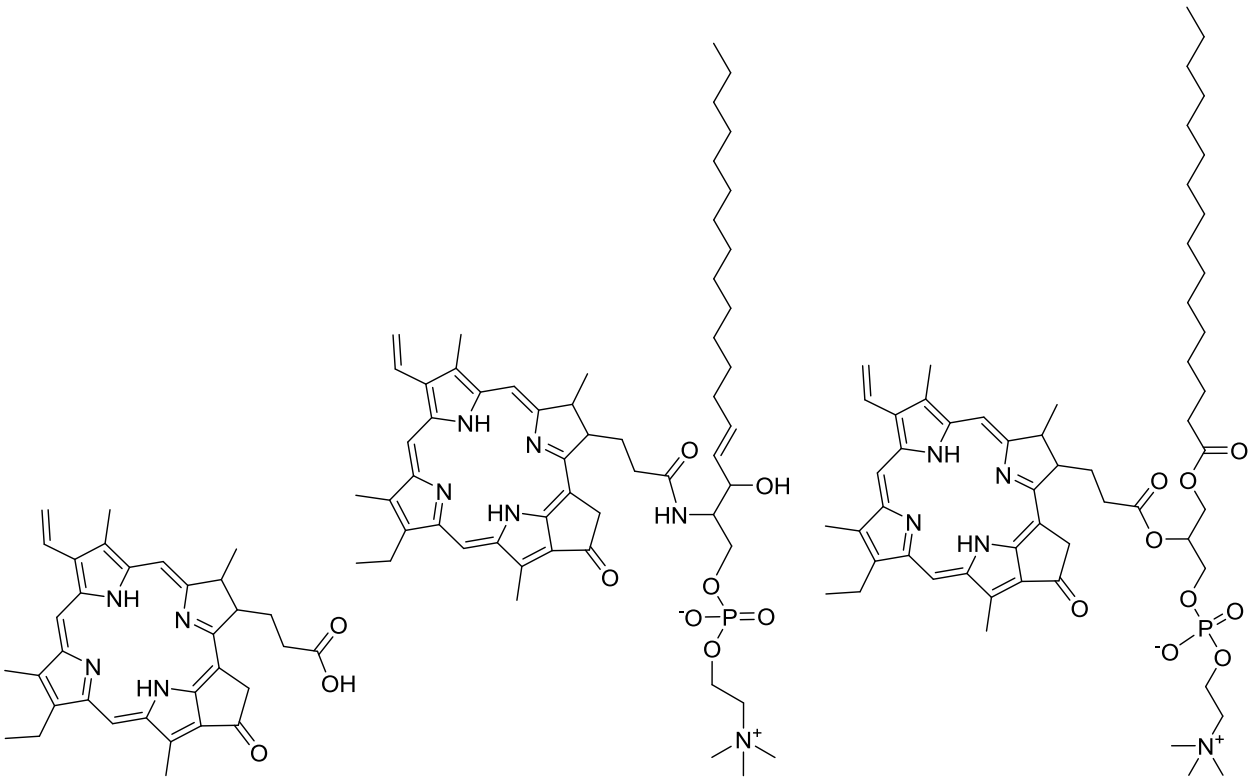

Figure 1: Chemical structures of pyropheophorbide-a and its lipid conjugates.

Results and Discussion

Interfacial Behavior of Pyropheophorbide a and its Conjugates

The two-dimensional phase behavior of the Pyro-a, PyroLPC and PyroLSM compounds at the air/buffer interface was studied by surface pressure measurements using Langmuir balance. The π-A isotherms obtained for Pyro-a and the two lipid-porphyrin conjugates (PyroLPC and PyroLSM) are shown in Figure 2. From these isotherms we estimated the molecular area at the surface pressure onset (A_0), the molecular area at surface pressure of 30 mN/m (A_{30}), the limit area (A_{limit}) which is obtained from the zero intersection by extrapolating the linear steep increase

of the surface pressure [19, 20] and the compressional modulus (K or Cs^{-1}). Their characteristic values are summarized in Table 1. Pyro-a monolayer displays similar isotherm characteristics as previously reported[11] with A_{limit} = 56 $Å^2$ and A_{30} = 47 $Å^2$. These small molecular areas correspond to the formation of closely packed films of Pyro-a molecules that exhibit side-on orientation while exposing the carboxyl group to the buffer subphase.

Table 1: The mean values (n=3) of the limit molecular area (A_{limit}), molecular area at surface pressure of 30 mN/m (A_{30}) and the maximal compressional modulus (K_{max}) for Pyro-a, PyroLPC, and PyroLSM monolayers. The standard errors of the molecular areas are for three trials.

Monolayer composition	**A_0 ($Å^2$)**	**A_{30} ($Å^2$)**	**A_{limit} ($Å^2$)**	**K_{max} (mN/m)**
Pyropheophorbide-a	69±4	48±1	57±2	190±26
PyroLPC	103±3	75±2	87±2	225±21
PyroLSM	80±3	63±2	70±2	394±31

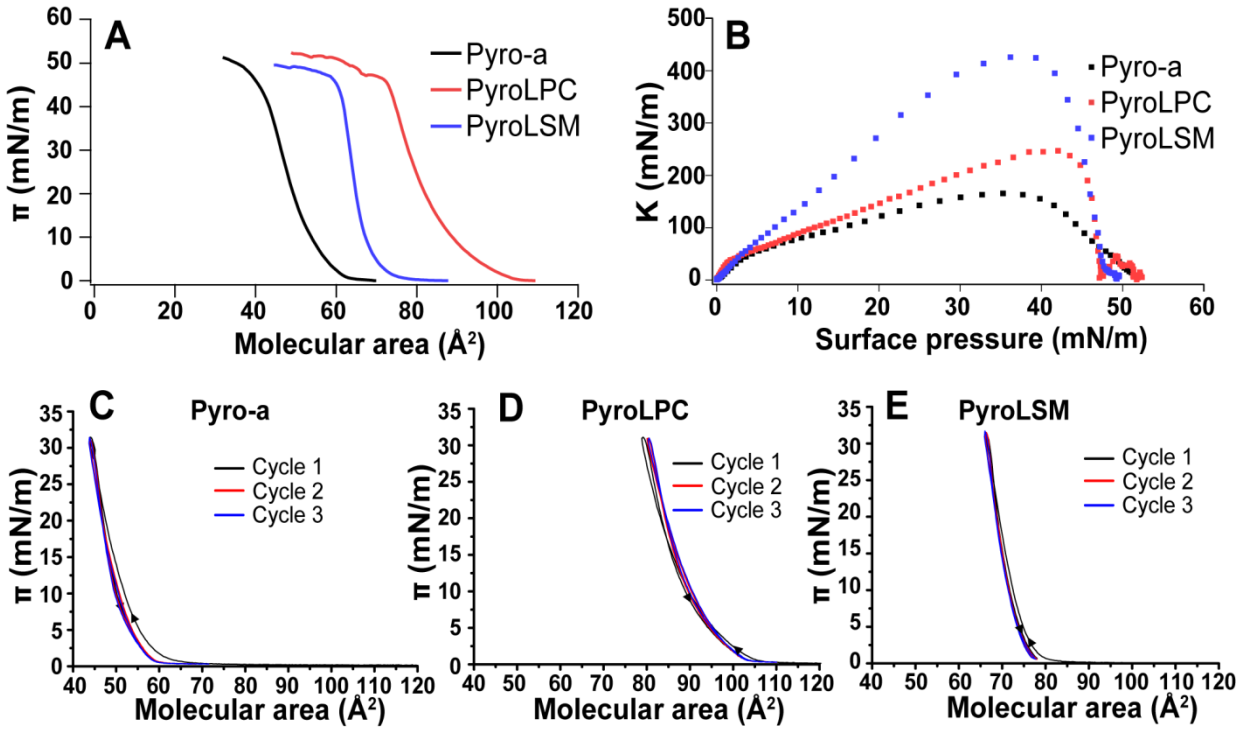

Figure 2: π-A isotherms of (A) and the corresponding compressibility modulus (B) for Pyro-a, PyroLSM and PyroLPC compounds spread on HEPES buffer. (C), (D), (E) are the compression-expansion cycles of Pyro-a, PyroLSM and PyroLPC monolayers respectively.

Compared to the Pyro-a, PyroLPC and PyroLSM conjugates showed significantly more expanded monolayers with A_{limit} values of 84 Å^2 and 70 Å^2, respectively. In addition, while the PyroLPC displayed π-A isotherm features similar to that of Pyro-a, PyroLSM exhibited a sharper phase transition between the gaseous and the liquid–condensed phase. These observations were further supported by the calculation of the compressional modulus (Eq. 1), where PyroLSM exhibited the highest maximal value (K_{max} = 425 mN/m) followed by that of PyroLPC (K_{max} = 247 mN/m) and Pyro-a (K_{max} = 166 mN/m), respectively. Such compressional modulus values indicate that the three compounds form monolayers in the liquid condensed state.[21] Whereas the molecular area expansion of the conjugates compared to Pyro-a can be explained by the presence of the

phosphatidylcholine headgroup in the vicinity of the porphyrin core, the difference in their compressional modulus implies different lateral packing between the molecules which is favored by the presence of LysoSM backbone for PyroLSM. Indeed, it has been demonstrated that sphingomyelins exhibit tighter interfacial packing compared to the chain-matched phosphatidylcholines.[22, 23] This was related to the presence of the interfacial hydroxyl and amide residues that promote the formation of hydrogen bonds with the surrounding molecules as previously reported by Steinbauer *et al.*[22] and Li *et al.*[23]. The stability of the monolayers as well as the reversibility of their two-dimensional surface phase transitions were assessed by subjecting the monolayers to three repetitive compression-expansion cycles (Figures 2C-E). The monolayers were first compressed to a surface pressure of 30 mN/m where a liquid-condensed phase is obtained and then expansed to zero surface pressure. Following the first expansion step, Pyro-a exhibited more significant hysteresis compared to PyroLSM and PyroLPC which indicates the higher lateral interaction between the Pyro-a molecules. Interestingly, the isotherms in the subsequent compression-expansion cycles were almost superimposed with a slight reduction in the limit molecular area ($A_{limit} < 5Å^2$), thus evidencing the reversibility and the stability of the three monolayers.

Brewster Angle Microscopy Analysis

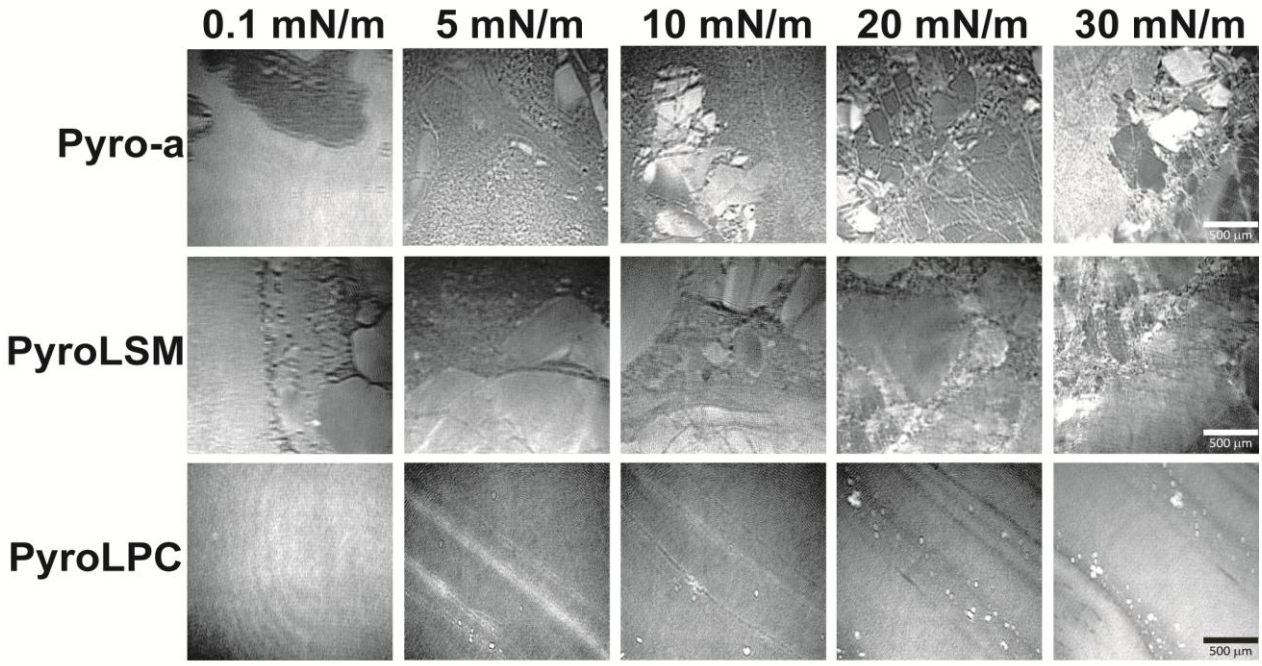

Figure 3: Representative BAM images for Pyro-a, PyroLSM and PyroLPC monolayers spread on HEPES buffer registered during compression at a temperature of 22±1°C. Scale bar corresponds to 500 µm.

The morphology of the monolayers of Pyro-a, PyroLPC and PyroLSM was assessed using Brewster angle microscopy and the images were recorded at increasing surface pressures (Figure 3). At the beginning of the monolayer compression (π = 0.1 mN/m), Pyro-a film appeared smooth with the presence of bright and dark regions which may be explained by the different molecular orientation relative to the incident p-polarized laser. As the surface pressure increases, the formation of bright island-like structures was observed and they grow gradually with the surface pressure up to 30 mN/m. The PyroLSM monolayer showed similar island-like structures but with bigger size that were present even at very low surface pressures (< 1 mN/m). Conversely,

PyroLPC monolayer exhibited smooth film during the whole compression which becomes brighter with the increase in surface pressure.

AFM Imaging of Langmuir-Blodgett Transferred Films

In order to get higher resolution of the monolayers morphology, the films made of Pyro-a and the conjugates were transferred at a surface pressure of 30 mN/m (liquid-condensed phase) onto mica substrates by the Langmuir-Blodgett technique and they were imaged afterwards by AFM at room temperature in air conditions (Figure 4). The topographic AFM images of Pyro-a film (Figure 4A) showed separate crystalline structures exhibiting leaf-like structures with an average height of ~ 1.4 nm (Figure 4 A, lower panel). Conversely, both PyroLSM and PyroLPC conjugates showed continuous monolayer with the formation of structured domains exhibiting scales-like and flakes-like structures respectively with an average height of 0.15 - 0.25 nm (Figure 4B, 4C).

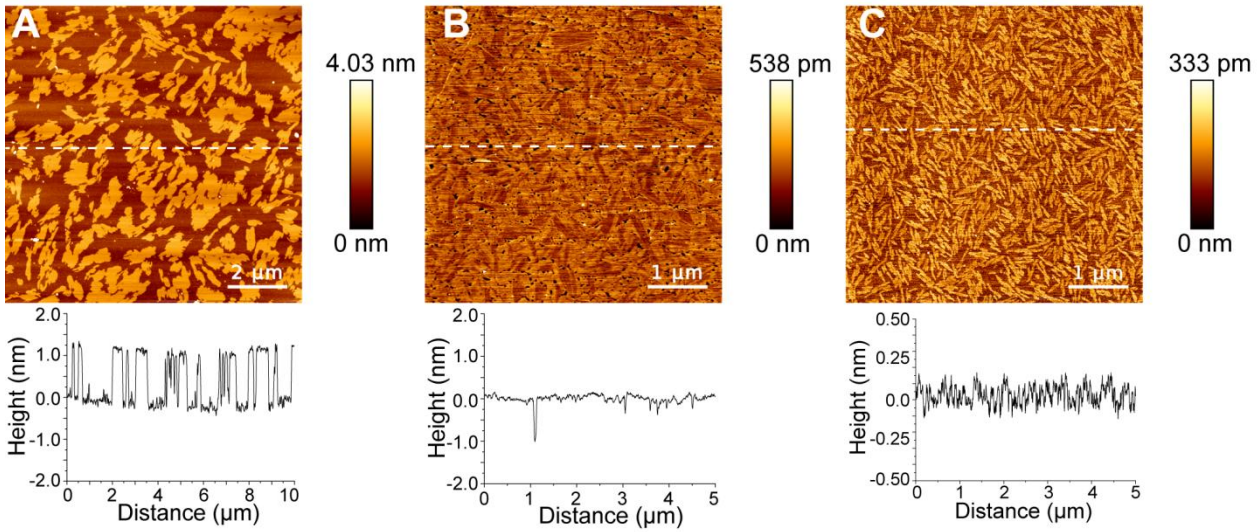

Figure 4:AM-AFM topography images in air of (A) Pyro-a, (B) PyroLSM and (C) PyroLPC compounds transferred on mica substrate at a surface pressure of 30 mN/m. The height profiles taken along the dashed lines are presented in the lower panels.

The Fine Structures Normal to the Interface of Pyro-a and Lipid-Porphyrin Conjugates Monolayers

The fine structures perpendicular to the plane of Pyro-A, PyroLSM and PyroLPC monolayers compressed to surface pressure of 30 mN/m were studied using specular X-ray reflectivity (XRR). Figures 4A shows the XRR curves of Pyro-a, PyroLSM and PyroLPC monolayers, fitted using a two-slabs model.[9, 11] The corresponding electron density profiles (ρ) reconstructed from the best fit results (solid black lines in Figures 4A) along the surface normal are shown in Figures 4B. The thickness (d), electron density (ρ) and root mean square roughness (σ) of each interface deduced from the best matching fits are summarized in Table 2. For the Pyro-a monolayer, the obtained total thickness is 16.4 Å, which is in agreement with the thickness of pheophorbide-a monolayer (thickness ~15.7 Å),[9] a porphyrin derivative with a similar structure to that of Pyro-a. In addition, this thickness value is consistent with the AFM height values and corresponds to the formation of Pyro-a film where the porphyrin molecules are stacked to each other with an upright orientation with the carboxyl group directed toward the water subphase. PyroLSM monolayer exhibits a total thickness of 19.3 Å. Such thickness is in agreement with that of similar compound named PhLSM[9, 10] which consists in grafting Pheo-a chromophore to LSM.

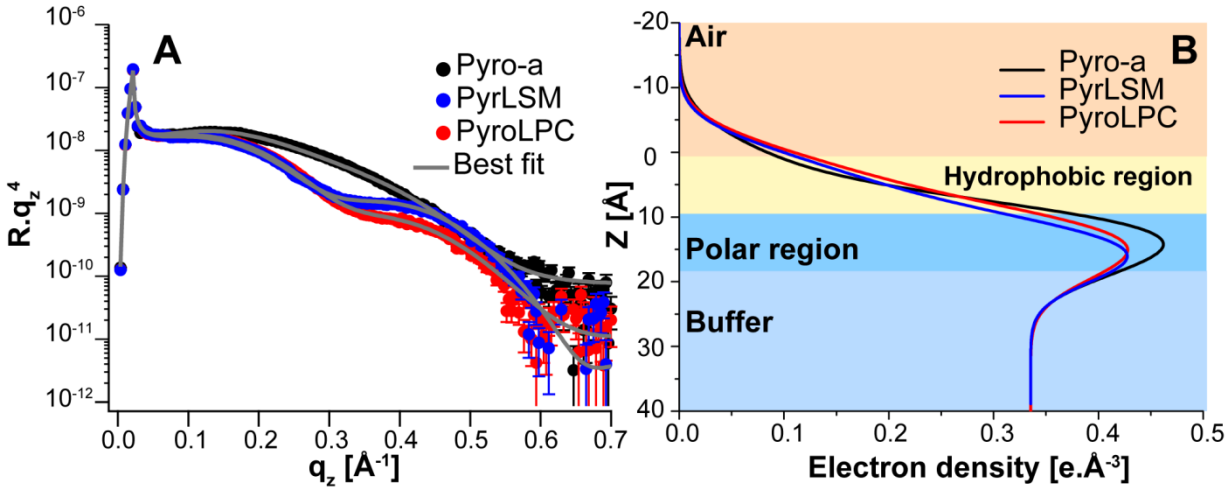

Figure 5: (A) XRR curves of Pyro-a, PyroLSM and PyroLPC monolayers on HEPES buffer at a surface pressure of 30 mN/m. The grey solid lines represent the best model fits to the experimental data. Error bars in the reflectivity data represent the statistical countingerrors. (B) The reconstructed electron density profiles along the Z-axis.

Compared to PyroLSM, the PyroLPC monolayer has a total thickness of 18.5 Å. This ~ 1 Å difference in the total thickness between the two Lipid-Por conjugates is mainly related to the structural difference between the lipid backbones. PyroLPC consists of a C16 Lyso-PC which is esterified in the sn2 position with the carboxylic group of the Pyro-a. However, PyroLSM has a LSM backbone which is consisting of a sphingosine chain of 18 carbons long. In addition, the interfacial hydroxyl group and amide residue of the sphingosine backbone could promote the formation of hydrogen bonds between the PyroLSM molecules thus leading to tighter packing with subsequent increase in the thickness. Similar behavior has been previously observed by Niemelä *et al.*[24] when comparing DPPC bilayer to that made of palmitoylsphingomyelin (PSM). By the mean of molecular dynamics simulations, the authors demonstrated that PSM molecules exhibit strong hydrogen bonding properties that led to specific ordering effects in the vicinity of

the polar headgroup with subsequent increase in the total thickness.[24] Besides, the electron density of the hydrophobic regions of the PyroLSM monolayer (ρ_{HC} = 0.194 e- × Å^{-3}) is lower than that of the PyroLPC (ρ_{HC} = 0.224 e- × Å^{-3}). Both lipid conjugates showed high electron densities in the polar region which could be related to the presence of the porphyrin core taking an upright orientation in the vicinity of the polar headgroup similar to other lipid-porphyrin conjugates.[11] However, it should be noticed that the electron density of the hydrophilic region of PyroLSM (ρ_{polar} = 0.481 e- × Å^{-3}) is higher than that of PyroLPC (ρ_{polar} = 0.467 e- × Å^{-3}). Such behavior could be explained by the structural differences in the polar headgroup causing a difference in the relative position of the porphyrin core at the air/buffer interface.

Table 2: Best fit parameters for the XRR Results for Pyro-a, PyroLSM and PyroLPC monolayers at 30 mN/m as presented in Figure 4.

	d (Å)	**ρ (e$^-$ × Å^{-3})**	**σ (Å)**
		Pyro-a	
Hydrophobic core	9.8±0.3	0.455±0.005	4.1±0.1
Choline group	6.6±0.4	0.389±0.007	3.4±0.2
Buffer	∞	0.335	5.6±0.2
		PyroLSM	
Hydrophobic core	10.3±0.2	0.194±0.009	4.5±0.2
Hydrophilic groups	9.0±0.3	0.481±0.008	4.2±0.2
Buffer	∞	0.335	3.6±0.1
		PyroLPC	
Hydrophobic core	9.0±0.2	0.224±0.012	4.9±0.2
Hydrophilic groups	9.5±0.3	0.467±0.010	4.2±0.3
Buffer	∞	0.335	3.5±0.3

Grazing Incidence Small Angle X-ray Scattering (GISAXS) Measurements

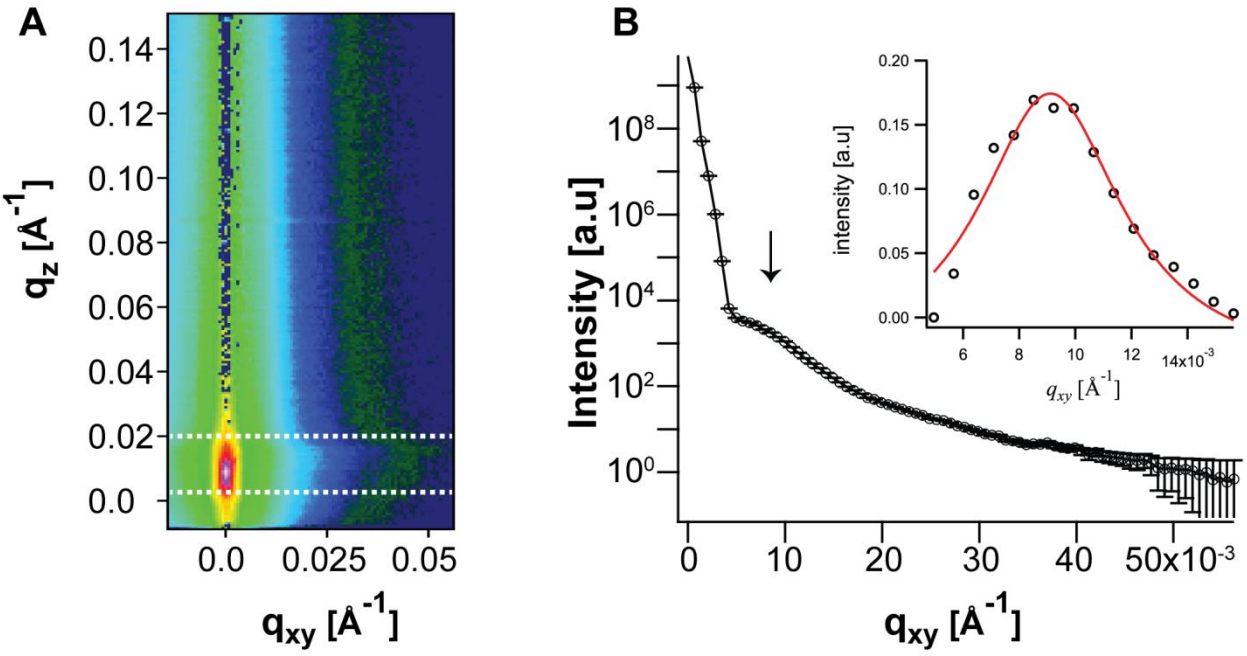

Figure 6. (a) GISAXS reciprocal space map of Pyro-a monolayer recorded at a surface pressure of π = 30 mN/m. (b) The scattered intensity profile integrated between the dashed lines plotted versus q_{xy}. The inset shows the GISAXS after subtracting an offset. The solid red line represents the least square fit with Gaussian.

To get further insight on the in plane lateral correlation between the domains imaged by AFM, grazing incidence small angle X-ray scattering (GISAXS) measurements (Figure S1) on the three monolayers were performed at a surface pressure of 30 mN/m. Whereas for PyroLPC and PyroLSM monolayers GISAXS signals could not be detected, a significant signal could be observed for Pyro-a film. This is due to the electron density contrast between the molecules and their surrounding. For instance, the electron density of Pyro-a obtained from XRR for the hydrophobic core is approximately two times higher the correspondings values of PyroLPC and PyroLSM monolayers (Table 2). Taking the average electron density for the whole monolayer

then only Pyro-a (ρ_{avg} = 0.428 $e^-/Å^3$) has a good contrast with respect to water while it is not the case for PyroLPC (ρ_{avg} = 0.349 $e^-/Å^3$) and PyroLSM (ρ_{avg} = 0.328 $e^-/Å^3$).Though the PyroLSM showed a weak GISAXS signal (Fig S2). Indeed, in the case of Pyro-a, molecules can interact with each other via face to face stacking but also via edge to edge interactions on both sides of each molecule. However in the case of the conjugates, due to the presence of a lipid backbone the interactions between the porphyrin cores will be limited which leads to the formation of smaller size domains. The GISAXS reciprocal space map is shown in **Figure 6A**. The intensity is integrated between the two dashed lines along q_{xy} and presented in **Figure 6B**. The intensity profile exhibits a peak as indicated by the arrow. In order to accurately determine the peak position, a linear offset is subtracted from the intensity profile and then it is fitted with Gaussian (inset, Figure 6B). The peak position is found to be located at q_{xy} = 0.0091 $Å^{-1}$ corresponding to inter-domain spacing of 69.1 nm. The correlation length can be estimated from the peak width using Scherrer formula as $L = \frac{0.9 \times 2\pi}{\Delta q_{xy}}$ *(Eq. 2)* where Δq_{xy} is the full-width at half maximum. The correlation length is estimated to be L = 111 nm which means that the interaction between the domains reach only up to the second neighbors. On the other hand, PyroLSM monolayer exhibited a weak GISAXS peak at q_{xy} = 0.0213 $Å^{-1}$ corresponding to inter-domain spacing of 29.5 nm which agrees very well with AFM results where the domains of PyroLSM is smaller to that of Pyro-a.

Conclusion

In this study, we demonstrated that Pyro-a and its lipids conjugates can form stable monolayers at the air/buffer interface. PyroLSM compounds formed a more condensed monolayer with lateral packing compared to the PyroLPC. This shed light on the impact of the lipid backbone on their organization. Indeed, from the X-Ray reflectivity data, we could determine that the Pyro-a

molecule take an upright orientation in the vicinity of the polar headgroup for both PyroLPC and PyroLSM. The compression of Pyro-a and its conjugates led to the formation of 2D domains at the air/water interface which size and shapes depended significantly on the chemical structure of the conjugate. The AFM topographic images revealed that Pyro-a molecules do not form homogenous film as the conjugates do. While Pyro-a monolayer compressed at 30 mN/m exhibited separated leaf-like structures, PyroLSM and PyroLPC ones displayed scales-like and flakes-like structures respectively. In addition, PyroLSM domains were larger than those of PyroLPC which could be attributed to an increase in the line tension for PyroLSM due to the higher van der Waals interactions offered by the LSM compared to LPC backbone. GISAXS signals were only detected for Pyro-a monolayer which could be due to the big size of domains. The GISAXS signals collected for Pyro-a at the air/buffer interface enabled the calculation of the inter-domain correlation length which was ~ 111 nm consistent with the AFM data. Taken together, our results demonstrated the significant impact of the lipid backbone on the lateral packing of the conjugates as well as on the shape and size of the formed domains. This could have a great impact on the photophysical properties of the conjugates when assembled into supramolecular structures. Indeed, both PyroLPC and PyroLSM conjugates can form liposome-like structures however due the significant difference in the lateral packing of the two conjugates, they may interact and orient differently in the lipid bilayer matrixes which in turn impacts their photophysical properties but also their stability in biological media.

Acknowledgements

LGB is thankful to the French Ministry of Research for the financial support of his PhD thesis. The financial supports for Lipid-Porphyrin conjugates research from the ANR JCJC Grant (ANR-19-CE09-0015 LISiNA) and from the Laboratory of Excellence LERMIT via an ANR grant

(ANR-10-LABX-33) under the program of ‘‘Investissements d’avenir’’ are gratefully acknowledged. This project has also received financial support from the CNRS through the MITI interdisciplinary programs. We thank the ESRF for the synchrotron beam time. We are also thankful to the CNRS to fund the exchange program between the CNRS and the university of Toronto under the 80 PRIME scheme.

References

[1] M. A. Rajora, J. W. H. Lou, G. Zheng, Chem. Soc. Rev. 2017, 46, 6433-6469.
[2] J. F. Lovell, C. S. Jin, E. Huynh, H. Jin, C. Kim, J. L. Rubinstein, W. C. Chan, W. Cao, L. V. Wang, G. Zheng, Nat. Mater. 2011, 10, 324-332.
[3] E. Huynh, G. Zheng, Nano Today 2014, 9, 212-222.
[4] C. S. Jin, J. F. Lovell, J. Chen, G. Zheng, ACS Nano 2013, 7, 2541-2550.
[5] J. F. Lovell, C. S. Jin, E. Huynh, T. D. MacDonald, W. Cao, G. Zheng, Angew. Chem., Int. Ed. Engl. 2012, 51, 2429-2433.
[6] I. Rizvi, G. Obaid, S. Bano, T. Hasan, D. Kessel, Lasers Surg. Med. 2018, 50, 499-505.
[7] G. Obaid, W. Jin, S. Bano, D. Kessel, T. Hasan, Photochem. Photobiol. 2019, 95, 364-377.
[8] J. Massiot, A. Makky, F. Di Meo, D. Chapron, P. Trouillas, V. Rosilio, Phys. Chem. Chem. Phys. 2017, 19, 11460-11473.
[9] J. Massiot, V. Rosilio, N. Ibrahim, A. Yamamoto, V. Nicolas, O. Konovalov, M. Tanaka, A. Makky, Chem. - Eur. J. 2018, 24, 19179-19194.
[10] J. Massiot, V. Rosilio, A. Makky, J. Mater. Chem. B 2019, 7, 1805-1823.
[11] L.-G. Bronstein, P. Cressey, W. Abuillan, O. Konovalov, M. Jankowski, V. Rosilio, A. Makky, J. Colloid Interface Sci. 2022, 611, 441-450.
[12] L.-G. Bronstein, Á. Tóth, P. Cressey, V. Rosilio, F. Di Meo, A. Makky, Nanoscale 2022, 14, 7387-7407.
[13] J. Massiot, W. Abuillan, O. Konovalov, A. Makky, Biochim. Biophys. Acta, Biomembr. 2022, 1864, 183812.
[14] J. M. Kroon, E. J. R. Sudhoelter, A. P. H. J. Schenning, R. J. M. Nolte, Langmuir 1995, 11, 214-220.
[15] C. Ponchut, J. M. Rigal, J. Clément, E. Papillon, A. Homs, S. Petitdemange, J. Instrum. 2011, 6, C01069-C01069.
[16] W. Abuillan, E. Schneck, A. Korner, K. Brandenburg, T. Gutsmann, T. Gill, A. Vorobiev, O. Konovalov, M. Tanaka, Phys. Rev. E 2013, 88, 012705.
[17] A. Nelson, J. Appl. Crystallogr. 2006, 39, 273-276.
[18] M. Veschgini, W. Abuillan, S. Inoue, A. Yamamoto, S. Mielke, X. Liu, O. Konovalov, M. P. Krafft, M. Tanaka, ChemPhysChem 2017, 18, 2791-2798.
[19] E. Chifu, J. Zsakó, M. Tomoaia-Cotişel, J. Colloid Interface Sci. 1983, 95, 346-354.
[20] M. Jurak, K. Szafran, P. Cea, S. Martín, Langmuir 2021, 37, 5601-5616.
[21] J. T. Davies, E. K. Rideal, Interfacial Phenomena, Academic Press: New York and London, 1963.

[22] B. Steinbauer, T. Mehnert, K. Beyer, Biophys. J. 2003, 85, 1013-1024.
[23] X. M. Li, M. M. Momsen, J. M. Smaby, H. L. Brockman, R. E. Brown, Biochemistry 2001, 40, 5954-5963.
[24] P. Niemelä, M. T. Hyvönen, I. Vattulainen, Biophys. J. 2004, 87, 2976-2989.

Twitter handles:

@Alimakky_LPCS, @umr8612

Table of contents (ToC) entry:

The impact of the lipid backbone structure on the interfacial behavior of lipid-porphyrin conjugates (PyroLSM and PyroLPC) monolayers has been investigated. By combining Langmuir balance to a variety of other physical techniques, we could demonstrate that the lipid backbone play an important role in controlling their lateral packing but also the shape and the size of formed domains.